

SCIPP-03/07

# The Most Likely Path of an Energetic Charged Particle Through a Uniform Medium

**D.C. Williams**

Santa Cruz Institute for Particle Physics, Santa Cruz, CA 95064, USA

E-mail: davidw@scipp.ucsc.edu

**Abstract.** Presented is a calculation of the most likely path for a charged particle traversing a uniform medium and suffering multiple-Coulomb scattering when the entrance and exit positions and angles are known. The effects of ionization energy loss are included and the results are verified using Monte Carlo simulation. The application to proton computed tomography is discussed.

PACS numbers: 87.53.Pb,87.57.Gg

## 1. Introduction

The use of protons in medical imaging (proton Computed Tomography or pCT) is not a new idea (Hanson *et al* 1982) and has recently gained more relevance due to the growing list of proton treatment centers and the limitations of proton treatment planning based on x-ray imaging (Schaffner and Pedroni 1998, Schneider and Pedroni 1995). One of the disadvantages of pCT is the tendency for protons to scatter in the target, thus blurring the image. This disadvantage can be alleviated by measuring the trajectory of individual protons using modern detector technology (Keeney *et al* 2002).

Detectors can measure the trajectory of a proton before entering and after leaving a target. No direct information is available while the proton is traveling within the target. Some type of extrapolation is therefore required for optimal pCT imaging. Because of the random nature of proton scattering, it is not possible to calculate the precise trajectory of the proton within the target, just the most likely path along with a probability envelope. The most likely path will asymptotically approach the entrance and exiting proton trajectories for points approaching the corresponding target surfaces.

This article presents a derivation of a simple, closed-form expression for the most likely path of a charged particle through material when the entrance and exit trajectories are known. The approach closely follows a previous derivation (Schneider and Pedroni 1994), except a  $\chi^2$  formalism is used which simplifies the calculation. The results are tested under various scenarios using detailed Monte Carlo simulation. The application to pCT image reconstruction is then discussed.

## 2. Hadron Treatment Planning and pCT

A conceptual design (Schulte *et al* 2003) of a pCT imaging device is shown in figure 1. The purpose of such a device is to measure both the entrance and exit angles and positions of individual protons, along with the exit energy. The single proton data would then be tabulated and presented to a computer for image reconstruction. Because the initial proton energy is well understood and constrained in a typical medical accelerator facility (see, for example, Coutrakon *et al* 1994), there is no need to measure the initial proton energy.

Choosing the proton energy for pCT is a balance between two tradeoffs. Lower momentum protons lose more relative energy providing higher image contrast. Higher momentum protons deposit less energy into the patient resulting in lower dosage. The optimal energy may not be known until prototype pCT devices can be tested, although kinetic energies between 200 and 250 MeV have been suggested for imaging of humans (Schulte *et al* 2003, Hanson *et al* 1982).

Medical imaging with pCT is particularly well suited to hadron therapy treatment planning. Such planning is typically performed using images from conventional x-ray computed tomography (XCT) after converting the x-ray absorption rate into equivalent hadron stopping power. Because such conversions depend on the atomic characteristics

of the material in the body, inaccuracies can be introduced (Scheider *et al* 1996), especially through places of high density (bone matter) or through foreign objects (metal plates or bolts). Because pCT employs proton stopping power directly in the image, pCT could remove much of this uncertainty.

An additional uncertainty in hadron treatment is the positioning of the patient in the accelerator in comparison to the images taken for treatment planning. One other possible advantage of pCT is the ability to image patients as they lay positioned in front of the accelerator just prior to treatment.

Reasonable goals for the accuracy of a pCT image for the purposes of hadron treatment planning is a spacial granularity of 1 mm and a density resolution of 1% (Schulte *et al* 2003). It will be difficult to achieve the former goal if the trajectory of protons in the patient cannot be predicted within this accuracy. Beyond these stated goals, any additional improvement in image quality will allow imaging using fewer protons, thus reducing patient dosage.

### 3. Multiple-Coulomb Scattering

Multiple-Coulomb scattering (MS) is the process that tends to scatter the direction of charged particles as they cross matter without changing their total momentum. Most high-energy physicists are familiar with this process since it is often the limiting factor in the performance of charged-particle detectors. A summary of this process can be found in the *Review of Particle Physics* from the Particle Data Group (Hagiwara *et al* 2002). The most relevant features are described here.

MS is a statistical process involving the sum of many individual elastic interactions between a charged particle and the nuclei of the matter traversed. Each individual nuclear interaction produces a complex distribution of scatter angles. However, after introducing many of these interactions, the combined result is a distribution that is fairly Gaussian. Because Gaussian distributions are simple to deal with, a Gaussian

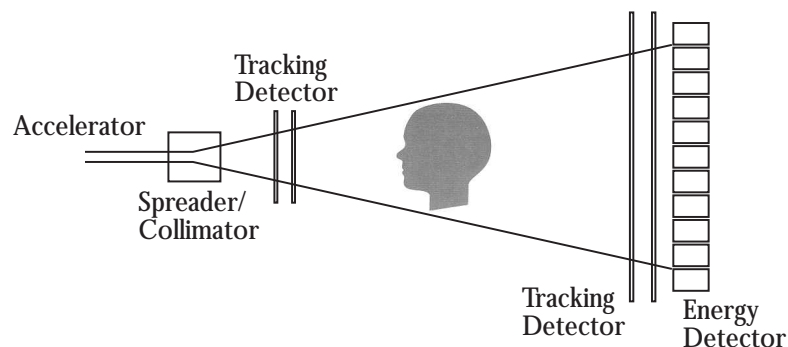


**Figure 1.** Conceptual design of a pCT detector. Tracking detectors measure the initial and exit position and angles of the proton. A calorimeter measures the exit energy.

approximation will be assumed in what follows. In this approximation, the amount of MS is characterized by the width  $\sigma_\theta$  of the Gaussian characterizing the distribution of scattering angles.

As consistent with the statistical nature of MS,  $\sigma_\theta$  is proportional to the square-root of the amount of material ( $x$ ) traversed. To a reasonable approximation, the characteristics of any material composition can be described by one proportionality constant, the radiation length  $X_0$ . The amount a particle of a given type and momentum will scatter through any material is proportional to the square-root of the amount of radiation lengths ( $x/X_0$ ) traversed by the particle:

$$\sigma_\theta \propto \sqrt{x/X_0}. \quad (1)$$

MS also tends to displace the trajectory of a particle. This is illustrated in figure 2. The distribution of displacements  $y$  also tend to form a Gaussian distribution. The width  $\sigma_y$  of this distribution is proportional to the distance  $x$  traversed through the material and  $\sigma_\theta$ :

$$\sigma_y = \frac{1}{\sqrt{3}}x\sigma_\theta. \quad (2)$$

For purely statistical reasons, the Gaussian random distributions describing  $y$  and  $\theta$  tend to be correlated. That is, if a large, positive value of  $y$  is observed, one will most likely observe a large, positive value of  $\theta$ . More specifically, the correlation coefficient  $\rho_{y\theta}$  between the  $y$  and  $\theta$  distributions is  $\sqrt{3}/2$ .

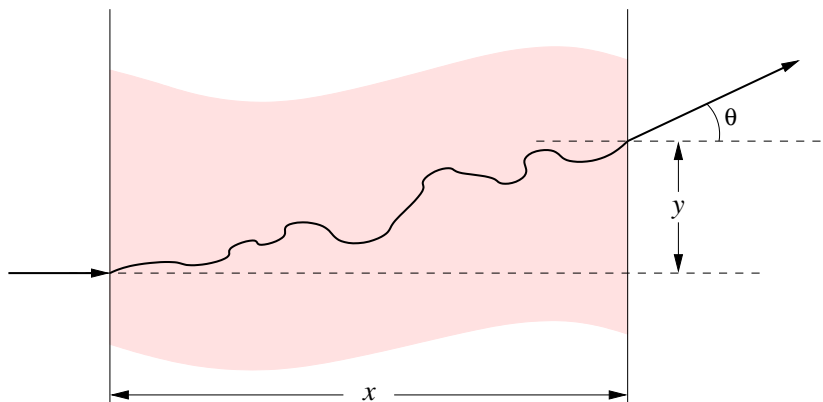


**Figure 2.** A diagram illustrating the scattering of a particle through a material of thickness  $x$  resulting in a displacement of  $y$  and a scattering angle of  $\theta$  (in one plane).

A particle can be deflected in any direction in two dimensions perpendicular to its path. For simplicity, this paper describes the scattering distribution projected onto one (arbitrary) plane. The scattering distribution in the orthogonal plane will have the same behavior (at least for a uniform material). The scattering in the two perpendicular planes is uncorrelated and can thus be treated independently. As a consequence, in practice, the equations presented in this paper will be used twice in a pCT image reconstruction program to account for scattering in both directions.

#### 4. Accounting for Energy Loss

Due to relativistic effects, the quantity  $\sigma_\theta$  is also inversely proportional to  $\beta p$ , where  $\beta = p/E$  is the velocity of the scattered particle,  $p$  is the total momentum, and  $E$  is the total energy. A completely accurate calculation of MS must take into account the loss of momentum of a particle (through a completely separate process called ionization energy loss) as it traverses the material. This correction is often neglected for high-energy particles because the relative loss of energy is small. This is not necessarily the case for pCT, in which case  $\sigma_\theta$  and  $\sigma_y$  are best calculated as the square root of an integral:

$$\sigma_\theta^2 = \Theta_0^2 \int_0^x \frac{1}{\beta^2 p^2} \frac{dx'}{X_0} \quad (3)$$

$$\sigma_y^2 = \Theta_0^2 \int_0^x \frac{(x-x')^2}{\beta^2 p^2} \frac{dx'}{X_0}, \quad (4)$$

where  $\Theta_0 \simeq 13.6 \text{ MeV}/c$  is a universal constant.

In the above integrals, the particle momentum  $p$  is calculated as a function of the distance  $x'$  it travels into the material. The functional form of  $p(x')$  can either be derived from equations governing ionization energy loss or taken from data or Monte Carlo simulation. For constant  $p$ , (3) and (4) simplify to (1) and (2).

#### 5. $\chi^2$ Estimator

We need to quantify how likely it would be for a particle to have scattered to a particular value of  $\theta$  and  $y$ . Since we are using a Gaussian approximation of MS, a  $\chi^2$  estimator is a convenient tool.

The  $\chi^2$  for correlated variables is calculated from the following linear equation:

$$\chi^2 = \delta_i \Delta_{ij}^{-1} \delta_j, \quad (5)$$

where  $\delta_i$  is the deviation of each variable from its measured value and  $\Delta_{ij}$  is the error matrix. For  $\theta$  and  $y$ , we have:

$$\Delta = \begin{pmatrix} \sigma_\theta^2 & \sigma_{\theta y}^2 \\ \sigma_{\theta y}^2 & \sigma_y^2 \end{pmatrix}, \quad (6)$$

where

$$\sigma_{\theta y}^2 = \Theta_0^2 \int_0^x \frac{x-x'}{\beta^2 p^2} \frac{dx'}{X_0} = \rho_{y\theta} \sqrt{\sigma_\theta^2 \sigma_y^2} \quad (7)$$

accounts for the correlation  $\rho_{y\theta}$  between the scattering angle  $\theta$  and the displacement  $y$ .

Combining (5) and (6) produces:

$$\chi^2(x, y, \theta) = \frac{\theta^2 \sigma_y^2 - 2\theta y \sigma_{\theta y}^2 + y^2 \sigma_\theta^2}{\det(\Delta)} \quad (8)$$

If energy loss is neglected ( $p(x) = \text{constant}$ ), (8) simplifies to

$$\chi^2(x, y, \theta) = \frac{4}{x \Theta_0^2} \left( \theta^2 - 3\theta y/x + 3y^2/x^2 \right). \quad (9)$$

## 6. Most Likely Path

Assume we have a particle that starts at position  $\{0, 0\}$  with zero angle and ends up, after traveling through material, at position  $\{x, y\}$  with angle  $\theta$ . The location of a particle at some intermediate point  $x_1$  is given by position  $y_1$  and angle  $\theta_1$ . This is illustrated in figure 3. We can solve (to first order in  $y$  and  $\theta$ ) for the most likely values of  $\theta_1$  and  $y_1$  using the  $\chi^2$  of (8):

$$\chi^2 = \chi^2(x_1, y_1, \theta_1) + \chi^2(x - x_1, y' - y_1, \theta_1 - \theta), \quad (10)$$

where the second  $\chi^2$  term is calculated from (8) using integrals from  $\{x_1, x\}$  and

$$y' \equiv y - (x - x_1) \sin \theta \quad (11)$$

is the projection of the final trajectory  $\{y, \theta\}$  onto the plane at  $x_1$ .

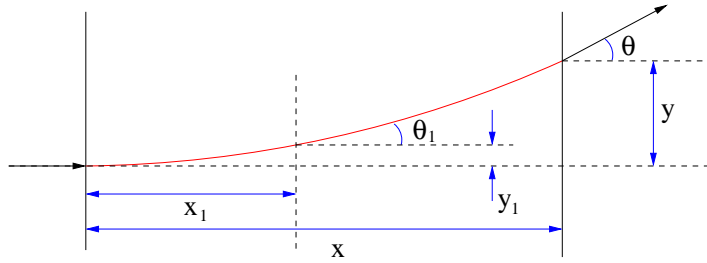


**Figure 3.** Definition of variables for the calculation of the most likely path of a particle.

The  $\{\theta_1, y_1\}$  minimum of this  $\chi^2$  for a given  $x_1$  can be calculated in the usual fashion:

$$\frac{\partial \chi^2}{\partial \theta_1} = \frac{\partial \chi^2}{\partial y_1} = 0. \quad (12)$$

This leads to the following solution for the most likely trajectory of the particle:

$$\theta_1(x_1) = \frac{CD - BE}{AC - B^2} \quad (13)$$

$$y_1(x_1) = \frac{AE - BD}{AC - B^2}, \quad (14)$$

where

$$A = \frac{\sigma_{y1}^2}{\det(\Delta_1)} + \frac{\sigma_{y2}^2}{\det(\Delta_2)} \quad (15)$$

$$B = -\frac{\sigma_{\theta y1}^2}{\det(\Delta_1)} + \frac{\sigma_{\theta y2}^2}{\det(\Delta_2)} \quad (16)$$

$$C = \frac{\sigma_{\theta1}^2}{\det(\Delta_1)} + \frac{\sigma_{\theta2}^2}{\det(\Delta_2)} \quad (17)$$

$$D = \frac{\theta \sigma_{y2}^2 + y' \sigma_{\theta y2}^2}{\det(\Delta_2)} \quad (18)$$

$$E = \frac{\theta \sigma_{\theta y2}^2 + y' \sigma_{\theta2}^2}{\det(\Delta_2)} \quad (19)$$

$$\det(\Delta_1) = \sigma_{\theta_1}^2 \sigma_{y_1}^2 - (\sigma_{\theta y_1}^2)^2 \quad (20)$$

$$\det(\Delta_2) = \sigma_{\theta_2}^2 \sigma_{y_2}^2 - (\sigma_{\theta y_2}^2)^2, \quad (21)$$

and where

$$\sigma_{\theta_1}^2 = \Theta_0^2 \int_0^{x_1} \frac{1}{\beta^2 p^2} \frac{dx'}{X_0} \quad (22)$$

$$\sigma_{y_1}^2 = \Theta_0^2 \int_0^{x_1} \frac{(x_1 - x')^2}{\beta^2 p^2} \frac{dx'}{X_0} \quad (23)$$

$$\sigma_{\theta y_1}^2 = \Theta_0^2 \int_0^{x_1} \frac{x_1 - x'}{\beta^2 p^2} \frac{dx'}{X_0} \quad (24)$$

$$\sigma_{\theta_2}^2 = \Theta_0^2 \int_{x_1}^x \frac{1}{\beta^2 p^2} \frac{dx'}{X_0} \quad (25)$$

$$\sigma_{y_2}^2 = \Theta_0^2 \int_{x_1}^x \frac{(x_1 - x')^2}{\beta^2 p^2} \frac{dx'}{X_0} \quad (26)$$

$$\sigma_{\theta y_2}^2 = -\Theta_0^2 \int_{x_1}^x \frac{x_1 - x'}{\beta^2 p^2} \frac{dx'}{X_0}. \quad (27)$$

Given that the path of a particle is determined from a  $\chi^2$  function whose minimum is a linear function in  $y_1$  and  $\theta_1$ , it follows that the probability of the particle leaving the most likely path is sampled from a Gaussian distribution. The  $\theta_1$  and  $y_1$  distributions will tend to be correlated and their combined two-dimensional Gaussian distribution can be described by the error matrix  $\sigma_{ij}^2$ , calculated from the inverse of the curvature matrix  $\alpha_{ij}$ :

$$\alpha_{ij}(x_1) \equiv \frac{1}{2} \frac{\partial^2 \chi^2}{\partial \delta_i \partial \delta_j} = \frac{1}{\Theta_0^2} \begin{pmatrix} A & B \\ B & C \end{pmatrix}. \quad (28)$$

The solution is:

$$\sigma_{ij}^2(x_1) = \frac{\Theta_0^2}{AC - B^2} \begin{pmatrix} C & -B \\ -B & A \end{pmatrix}. \quad (29)$$

For example, the width  $\sigma_{y_1}(x_1)$  of the Gaussian describing the distribution of  $y_1(x_1)$  is equal to:

$$\sigma_{y_1}(x_1) = \Theta_0 \sqrt{\frac{A}{AC - B^2}}. \quad (30)$$

## 7. Demonstration with Geant4

The Geant4 simulation toolkit (Agostinelli *et al* 2003) is a general purpose computer library for the simulation of particles interacting with matter. Developed initially for applications within the high-energy physics community, Geant4 has since found acceptance in the astronomy and medical fields, among others. Included among the many physical processes implemented in Geant4 is a sophisticated non-Gaussian model of MS whose accuracy has been verified with experimental data. It is therefore an ideal tool in which to test the derivations reported in this paper.

**Table 1.** Monte Carlo test conditions. The amount of material traversed in all cases was 20 cm.

	Beam energy	Material	Mean exit energy (MeV)	Number Protons	
	(MeV)			Generated	Exited
(a)	200	water	$87 \pm 2$	1010	1010
(b)	400	water	$337 \pm 1$	1010	1010
(c)	300	compact bone	$157 \pm 2$	1010	1009

Three different conditions were tested using geant4 (see table 1): (a) 200 MeV protons through 20 cm of water, corresponding to nominal pCT conditions; (b) 400 MeV protons through 20 cm of water, to test the calculation at higher energies; and (c) 300 MeV protons through 20 cm of compact bone equivalent (ICRU 1984), to test the calculation with denser material. Generic models of hadronic interactions (from geant4 novice example 2, including both elastic and inelastic effects) were included in the simulation. A total of 1010 protons were generated under each condition. The first 1000 of the protons to survive passing through the material were used in the studies shown here.

The integrals of (3), (4), and (7) require a parameterization of the behavior of the quantity  $1/\beta^2 p^2$  as a function of penetration depth  $x$ . For the three test conditions presented here, this behavior can be extracted from the geant4 simulation, as shown in figure 4. For the purposes of calculating the integrals, the average  $1/\beta^2 p^2$  behavior from geant4 has been fit to a sixth order polynomial  $P_6$ :

$$P_6(x) = \sum_{i=0}^5 a_i x^i . \quad (31)$$

The results are shown in figure 4 and listed in table 2. The  $1/\beta^2 p^2$  behavior, in combination with the radiation length, can be used to predict  $\sigma_\theta$ ,  $\sigma_y$ , and  $\rho_{y\theta}$  at the proton exit position ( $x = 20$  cm). The radiation length of water ( $X_0 = 36.1$  cm) is well established (Hagiwara *et al* 2002). An approximate value for the radiation length of compact bone ( $X_0 = 16.6$  cm) can be calculated from the inverse of the weighted average of  $1/X_0$  from each of the composite elements. As shown in table 3, the calculations agree with the values obtained from geant4 within a few percent.

The polynomial fit to  $1/\beta^2 p^2$  shown in figure 4 can also be used to calculate the most likely proton path from the integrals of (22)–(27). The result of this calculation for test condition (a) and for several example exit positions and angles is shown in figure 6. In all cases, the most likely path is a smooth curve which tends to minimize the total amount of bending in the material. Results for test conditions (b) and (c) are similar.

Shown in figure 7 is the most likely path for four example exit angles and positions  $\{\theta, y\}$  and the corresponding one and two sigma envelopes for test condition (a). Due to ionization energy loss, protons tend to scatter more as they penetrate material, and so the envelope is somewhat larger nearer the exit position.



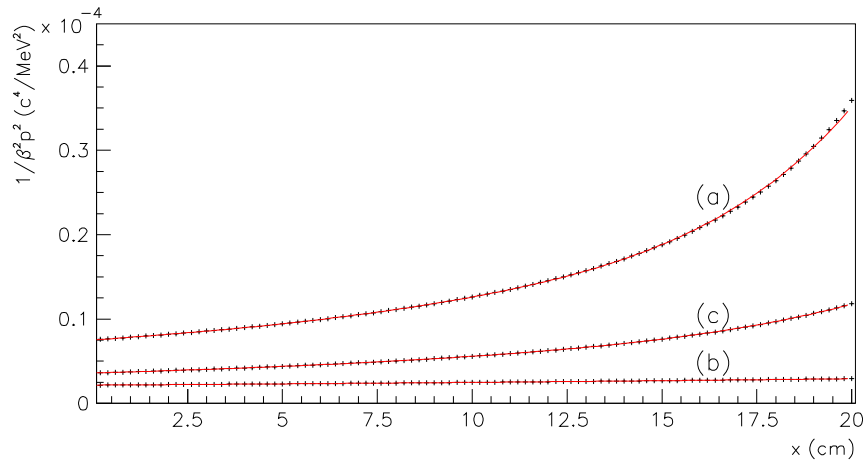


**Figure 4.** The average value of the quantity  $1/\beta^2 p^2$  as a function of penetration depth  $x$  for the three test conditions (a), (b), and (c) listed in table 1. The curves are fits to a sixth order polynomial.

**Table 2.** Results of the polynomial fit to the average value of  $1/\beta^2 p^2$  as a function of penetration depth, for the three test conditions. The units are  $c^2/\text{MeV}$  divided by various powers of cm.

	(a)	(b)	(c)
$a_0$	$7.507 \times 10^{-4}$	$2.160 \times 10^{-4}$	$3.596 \times 10^{-4}$
$a_1$	$3.320 \times 10^{-5}$	$2.858 \times 10^{-6}$	$1.340 \times 10^{-5}$
$a_2$	$-4.171 \times 10^{-7}$	$3.618 \times 10^{-8}$	$1.977 \times 10^{-7}$
$a_3$	$4.488 \times 10^{-7}$	$3.153 \times 10^{-10}$	$7.321 \times 10^{-8}$
$a_4$	$-3.739 \times 10^{-8}$	$1.939 \times 10^{-11}$	$-5.000 \times 10^{-9}$
$a_5$	$1.455 \times 10^{-9}$	$-3.161 \times 10^{-13}$	$2.136 \times 10^{-10}$

**Table 3.** The parameters describing the MS of protons under the three test conditions of table 1. The values presented without errors are predictions from (6). The values presented with errors are sampled from Monte Carlo.

	$\sigma_\theta$ (radian)	$\sigma_y$ (cm)	$\rho_{y\theta}$
(a)	0.0393	0.368	0.80
	$0.0389 \pm 0.0007$	$0.370 \pm 0.008$	$0.80 \pm 0.02$
(b)	0.0160	0.178	0.85
	$0.0175 \pm 0.0003$	$0.188 \pm 0.004$	$0.87 \pm 0.02$
(c)	0.0373	0.368	0.82
	$0.0400 \pm 0.0008$	$0.394 \pm 0.008$	$0.82 \pm 0.02$

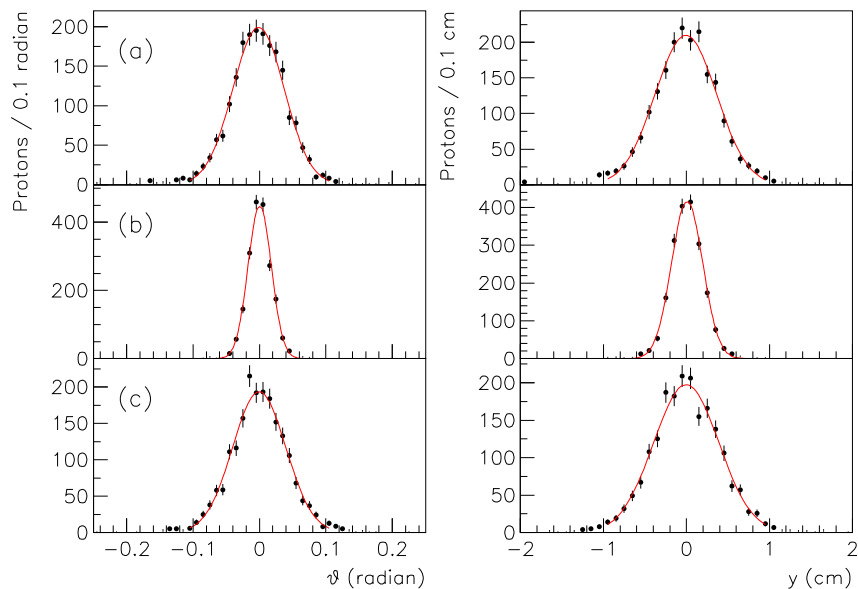


**Figure 5.** The distribution of  $\theta$  (left column) and  $y$  (right column) at  $x = 20$  cm for the three test conditions of table 1. Overlaid are fits to a Gaussian distribution used to produce the  $\sigma_\theta$  and  $\sigma_y$  values shown in table 3.

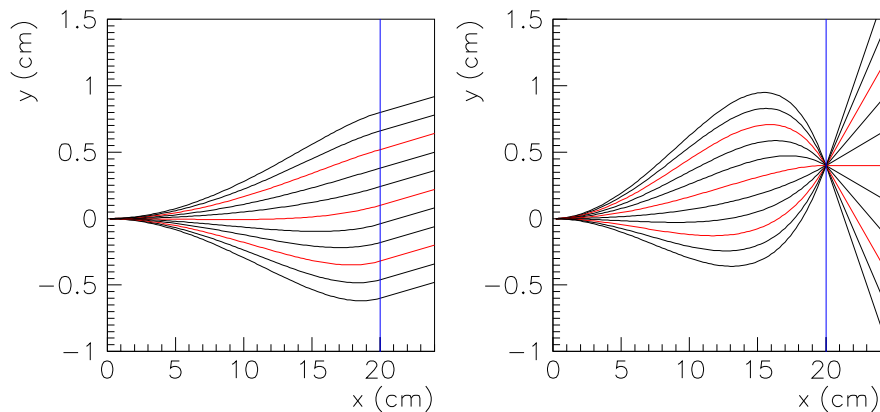


**Figure 6.** Examples of most likely paths as calculated using (14) for protons with initial kinetic energy of 200 MeV traveling through 20 cm of water. Each curve represents a separate calculation for each of the trajectories indicated by the straight lines drawn to the right of the vertical line.

The validity of (30) can be checked using the Geant4 simulation. To do so, the resulting final position and angle of each simulated proton is used to calculate the most likely path  $y_1(x_1)$  and the associated error  $\sigma_{y_1}(x_1)$ . The distribution of the deviation  $\delta_y = y_1 - y_1(x_1)$  from the predicted path is then sampled. If the calculation of  $y_1(x_1)$  and  $\sigma_{y_1}(x_1)$  is correct, the width of the  $\delta_y$  distribution should agree with  $\sigma_{y_1}(x_1)$ . This is indeed the case, within a few percent, for the simulations using water, as shown in figure 8. For compact bone, geant4 predicts a MS envelope that is approximately 5% larger, which is consistent with the results shown in table 3.

## 8. Application to pCT

To represent an image, CT typically divides a subject into an array of voxels by subdividing three-dimensional space with grids along the three cartesian axes. The image is represented by the average density contained in each voxel. To accurately reconstruct a pCT image, the calculated proton trajectory is used to decide which voxels an individual proton intersect and thus those voxels which contribute to the total proton energy loss. The size of the voxels determine the spacial resolution of the image. To obtain a resolution of 1 mm requires a voxel dimension at least that small.

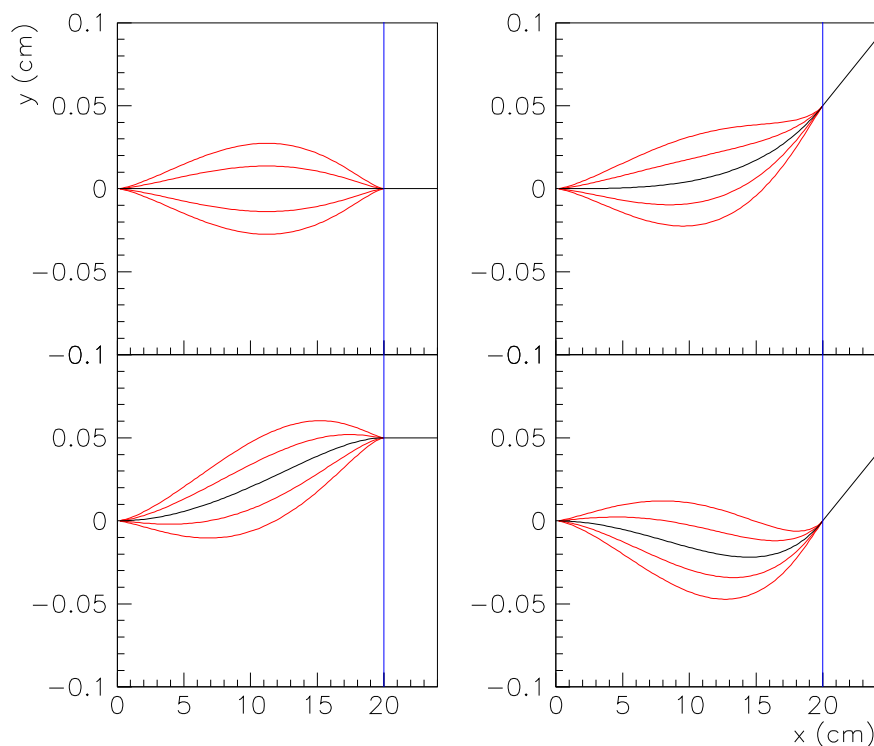


**Figure 7.** Example one and two sigma envelopes containing the most likely path of a particle of given exit position and angle for protons with initial kinetic energy of 200 MeV traveling through 20 cm of water.

As shown in figure 8, the path predicted by (14) is accurate to better than 1 mm for nominal pCT conditions. This appears sufficient enough for hadron therapy treatment planning, although higher accuracies will always be welcome to further improve the image or for other possible pCT applications. Nevertheless, it is an interesting exercise to compare the complete calculation to a simple approximation, such as a cubic spline:

$$\begin{aligned} y_1(x_1) &\approx c_2 x_1^2 + c_3 x_1^3 & (32) \\ c_2 &= 3y/x^2 - \theta/x \\ c_3 &= -2y/x^3 + \theta/x^2, \end{aligned}$$

where  $c_2$  and  $c_3$  are chosen to match the slope and position of the exiting proton. A comparison of this approximation and the full calculation for two example proton exit trajectories is shown in figure 9. In both cases the cubic spline is a reasonable approximation. Shown in figure 10 is the width  $\sigma_y$  of the deviation from the calculated trajectory for the simulation including water and a 200 MeV beam. The degradation in accuracy is approximately 8%.

Approximations like a cubic spline, however, do not provide an estimate of the width

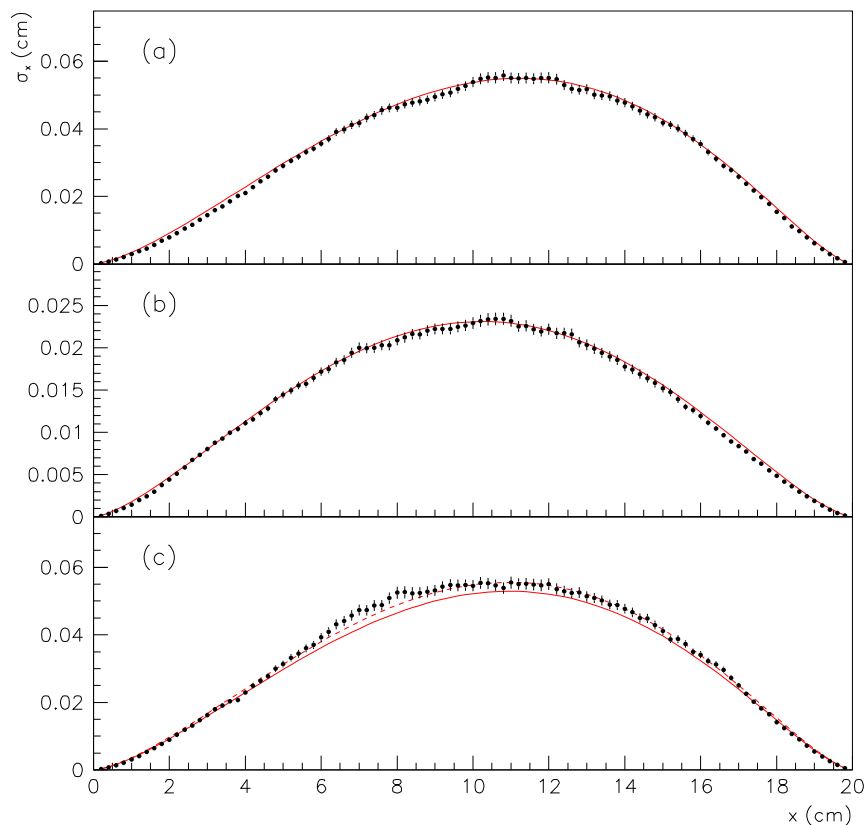


**Figure 8.** The width of the distribution  $\delta_y$  of the deviation from the predicted path (points) versus the predicted value (line), for the three test cases listed in table 1. The dotted line for (c) is the prediction for a value of  $X_0$  that is 5% smaller.

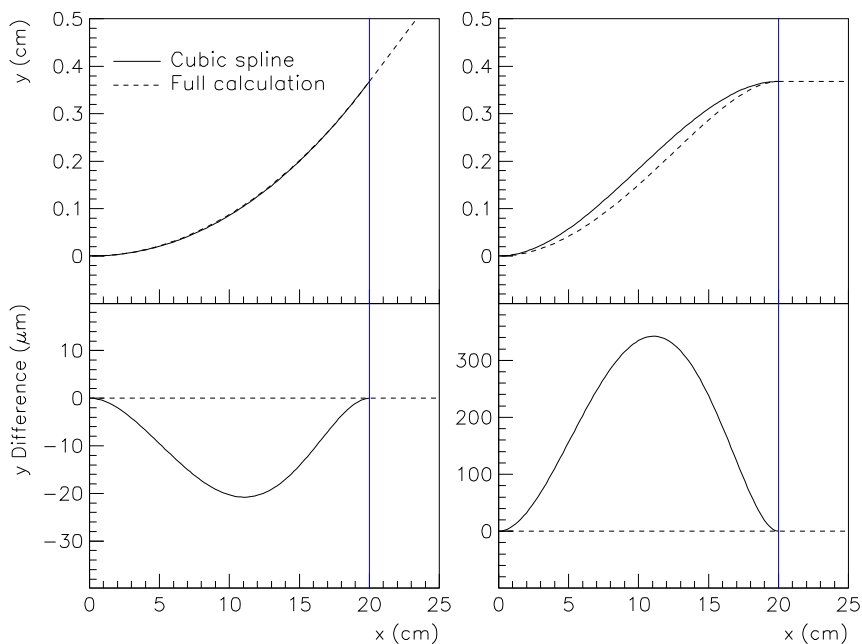


**Figure 9.** A comparison of the full trajectory calculation and a simple cubic spline, for protons with initial kinetic energy of 200 MeV traveling through 20 cm of water. Shown is the trajectory for a proton exit angle of one standard deviation (left) and zero exit angle (right) along with a proton exit position of one standard deviation. The lower plots are the difference of the two calculations.

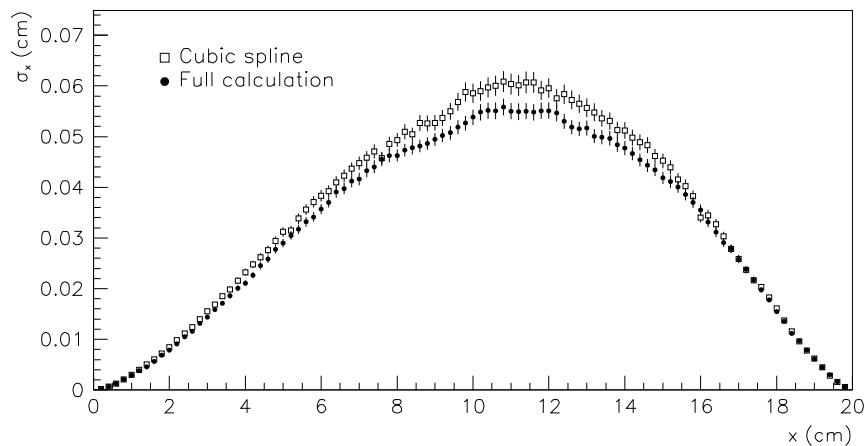


**Figure 10.** The width of the distribution  $\delta_y$  of the deviation from the predicted path for the full calculation and a cubic spline approximation, for protons with initial kinetic energy of 200 MeV traveling through 20 cm of water.

$\sigma_{y1}(x_1)$  of the distribution of possible trajectories. The width can be an important ingredient in image reconstruction. For example, an algorithm might integrate the trajectory likelihood over the volume of each voxel near the proton trajectory. Another possibility is to weight the contribution of a proton trajectory to a voxel solution by some function of the number of standard deviations the center of the voxel lies from the trajectory.

The use of the Gaussian approximation to MS simplifies the description of the trajectory envelope. Fortunately, as is evident from figure 5, the Gaussian approximation is fairly accurate. Depending on the image reconstruction algorithm, it may be necessary to treat the small non-Gaussian tails in some fashion, perhaps by discarding the data from those protons that exhibit large deflection or displacement.

The effect of inelastic nuclear interactions on the range of protons in hadron therapy has been well documented and can be significant (Medin and Andreo 1997). In the application for pCT, in which the proton travels through the subject and exits with significant energy remaining, the effect of inelastic hadronic interaction is minor. If a proton is lost, it will not be detected by the detectors behind the subject and will be ignored. If proton remnants exit the image subject, they do so at low energy and can easily be identified.

Although pCT is mostly immune to the effects of inelastic interactions, and such immunity ensures the accuracy of the calculations presented in this paper, the consequence is that an effect which is important to hadron therapy does not influence pCT images. This somewhat reduces the benefits of pCT in hadron therapy planning (with respect to XCT) as discussed earlier, especially if the inelastic cross section varies significantly between various tissues.

The MS formalism described in this paper has been applied to uniform material. In practice, pCT is used to image a subject that is non-uniform. As discussed earlier, the size of MS in each material is characterized by the associated radiation length. To apply the MS formulas to a particle traversing an object which is non-uniform in either composition or density, the radiation length  $X_0$  can be specified as a function of  $x_1$ . This function can be naturally incorporated into the integrals of (22)–(27).

Some caution must be observed. For granular non-uniformities in which small changes in trajectory result in substantial changes in material, the Gaussian approximation to MS will begin to break down. Because the width of the proton trajectory probability envelope is fairly small, the changes in densities must be abrupt to be noticeable, and if produced by small structures, will tend to have little effect on average. The exception are large objects that have a small dimension perpendicular to the beam (for example, a proton trajectory grazing the surface of a bone plate). Image reconstruction programs may need to apply special algorithms in such cases.

Rather than just a nuisance, the effect of non-uniformities on MS scattering can be used to advantage. Although pCT image reconstruction strategies have focused (in analogy to XCT) on the average proton energy loss to provide most of the image information, the proton scattering angle may also be useful. In particular, a change

in density in the subject not only produces higher proton energy loss, but produces higher proton MS angles. The measured angular distribution, combined with the MS predictions incorporated in the integrals (22)–(27) as discussed above, can be used to further improve image quality.

## 9. Conclusion

Using a Gaussian approximation of MS and a  $\chi^2$  formalism, it is possible to construct from first principles a closed-form expression for the most likely trajectory of a particle in a uniform material. This technique also provides the probability of the particle to deviate from this path. The important effect of energy loss can be incorporated into this calculation by introducing integrals involving the value of  $1/\beta^2 p^2$  for the particle as it traverses the material.

The results of the calculation are compared to a Monte Carlo simulation based on the Geant4 toolkit under a variety of conditions associated with pCT. Good agreement is observed.

## 10. Acknowledgements

The author would like to thank his colleagues in the pCT collaboration for their encouragement and invaluable advice.

## References

- Agostinelli S *et al* 2003 (GEANT4) Geant4—a simulation toolkit *Nucl. Instrum. Methods* **A506** 250
- Coutrakon G, Hubbard J, Johannng J, Maudsley G, Slaton T and Morton P 1994 A performance study of the Loma Linda proton medical accelerator *Med Phys.* **11** 1691
- Hagiwara K *et al* 2002 (Particle Data Group) The review of particle physics *Phys. Rev.* **D66** 010001
- Hanson K M, Bradbury J N, Koeppe R A, Macek R J, Machen D R, Morgado R, Paciotti M A, Sandford S A and Steward V W 1982 Proton computed tomography of human specimens *Phys. Med. Biol.* **27** 25
- Keeney B, Bashkirov V, Johnson R P, Kroeger W, Ohyama H, Sadrozinski R W M, Shulte R, Seiden A and Spradlin P 2002 A silicon telescope for applications in nanodosimetry *IEEE Tran. Nucl. Sci.* **49** (2002) 1724
- ICRU 1984 Stopping powers for electrons and positrons *Report 37*, International Commission on Radiation Units and Measurements, Bethesda MD
- Medin J and Andreo P 1997 Monte Carlo calculated stopping-power ratios, water/air, for clinical proton dosimetry (50-250 MeV) *Phys. Med. Biol.* **42** 89
- Schaffner B and Pedroni E 1998 The precision of proton range calculations in proton radiotherapy treatment planning: experimental verification of the relation between CT-HU and proton stopping power *Phys. Med. Biol.* **43** 1579
- Schneider U and Pedroni E 1994 Multiple Coulomb scattering and spatial resolution in proton radiography *Med. Phys.* **21** 1657
- 1995 Proton radiography as a tool for quality control in proton therapy *Med. Phys.* **22** 353
- Schneider U, Pedroni E and Lomax A (1996) The calibration of CT Hounsfield units for radiotherapy treatment planning *Phys. Med. Biol.* **41** 111

Schulte R *et al* 2003 Design of a Proton Computed Tomography System for Applications in Proton Radiation Therapy *to appear in IEEE Trans. Nucl. Sci.*